Plant Physiology®

Plant Physiology, 2024, **00**, 1–16
https://doi.org/10.1093/plphys/kiae284
Advance access publication 16 May 2024
Research Article

ELONGATED HYPOCOTYL 5 interacts with HISTONE DEACETYLASE 9 to suppress glucosinolate biosynthesis in *Arabidopsis*

Dasom Choi,[1] Seong-Hyeon Kim,[2] Da-Min Choi,[2] Heewon Moon,[1] Jeong-Il Kim,[2] Enamul Huq,[3] and Dong-Hwan Kim[1,*]

[1]Department of Plant Science and Technology, Chung-Ang University, Anseong 17546, Republic of Korea
[2]Department of Integrative Food, Bioscience and Biotechnology, Chonnam National University, Gwangju 61186, Republic of Korea
[3]Department of Molecular Biosciences, University of Texas at Austin, Austin, TX 78712, USA
*Author for correspondence: dhkim92@cau.ac.kr
The author responsible for distribution of materials integral to the findings presented in this article in accordance with the policy described in the Instructions for Authors (https://academic.oup.com/plphys/pages/General-Instructions) is Dong-Hwan Kim (dhkim92@cau.ac.kr).

Abstract

Glucosinolates (GSLs) are defensive secondary metabolites produced by *Brassicaceae* species in response to abiotic and biotic stresses. The biosynthesis of GSL compounds and the expression of GSL-related genes are highly modulated by endogenous signals (i.e. circadian clocks) and environmental cues, such as temperature, light, and pathogens. However, the detailed mechanism by which light signaling influences GSL metabolism remains poorly understood. In this study, we found that a light-signaling factor, ELONGATED HYPOCOTYL 5 (HY5), was involved in the regulation of GSL content under light conditions in *Arabidopsis* (*Arabidopsis thaliana*). In *hy5-215* mutants, the transcript levels of GSL pathway genes were substantially upregulated compared with those in wild-type (WT) plants. The content of GSL compounds was also substantially increased in *hy5-215* mutants, whereas 35S::*HY5-GFP*/*hy5-215* transgenic lines exhibited comparable levels of GSL-related transcripts and GSL content to those in WT plants. HY5 physically interacts with HISTONE DEACETYLASE9 and binds to the proximal promoter region of *MYB29* and *IMD1* to suppress aliphatic GSL biosynthetic processes. These results demonstrate that HY5 suppresses GSL accumulation during the daytime, thus properly modulating GSL content daily in *Arabidopsis* plants.

Introduction

Plants produce diverse natural defense compounds to cope with abiotic (e.g. drought and heat stress) and biotic (e.g. insects and pathogens) challenges. Among these compounds, glucosinolates (GSLs) are some of the most studied plant metabolites because of their agricultural importance as defense molecules and their human health-promoting benefits (i.e. anticarcinogenic and antimicrobial effects) (Hecht 2000; Fahey et al. 2012; Fuentes et al. 2015). GSLs are nitrogen- and sulfur-containing anionic secondary metabolites that can be classified into 3 subgroups according to their amino acid precursors: aliphatic (i.e. ethionine-, alanine-, leucine-, isoleucine-, valine-, or glutamate-derived), indolic (i.e. tryptophan-derived), and benzyl (i.e. phenylalanine- or tyrosine-derived) (Augustine and Bisht 2015).

Genes responsible for individual enzymatic steps in the GSL biosynthetic pathways have been identified in studies using *Arabidopsis* (*Arabidopsis thaliana*) model plants (Fig. 1). The biosynthetic pathways of GSLs comprise 3 major phases: (i) chain elongation, (ii) core structure formation, and (iii) side-chain modification (Sonderby et al. 2010). In the case of aliphatic GSL biosynthesis, the "chain elongation" phase starts with the deamination of a precursor amino acid (i.e. methionine), which is catalyzed to a 2-keto acid by the activity of BRANCHED-CHAIN AMINO ACID TRANSFERASE 4 (BCAT4) (Schuster et al. 2006). Next, the 2-keto acid is transported to the chloroplast organelle for subsequent steps via the activity of BILE ACID TRANSPORTER 5 (BAT5) (Farquharson 2009; Mitreiter and Gigolashvili 2021). Within the chloroplast, 2-keto acid undergoes a series of processes, including condensation, isomerization, and oxidative decarboxylation. These sequential catalytic reactions are conducted by methylthioalkyl malate synthases (MAMs), isopropylmalate isomerases (IPMIs), and isopropylmalate dehydrogenases (Petersen et al. 2019).

After the transamination reaction by BCAT3 in the chloroplast, the processed 2-keto acid is transferred to the "core structure formation" phase (Halkier and Gershenzon 2006). This phase of aliphatic GSL synthesis begins with 2 cytochrome P450 monooxygenase family proteins, CYTOCHROME P450 FAMILY 79F1 (CYP79F1) and CYP79F2, which convert 2-oxo acid into aldoximes that are further converted to nitrile oxide compounds by the oxidizing activity of CYP83A1. The product is then conjugated with glutathione by GLUTATHIONE S-TRANSFERASE F11 (GSTF11) and GLUTATHIONE S-TRANSFERASE TAU 20 (GSTU20) to form S-alkylthiohydroximate and further cleaved by GAMMA-GLUTAMYL PEPTIDASE 1 (GGP1). Next, SUPERROOT 1 (SUR1) encoding a C–S lyase enzyme converts S-alkylthiohydroximate to thiohydroximate (Halkier and Gershenzon 2006). Next, the thiohydroximate undergoes glycosylation by UDP-GLUCOSYLTRANSFERASE 74 B1 (UGT74B1) and sulfation by DESULFO-GLUCOSINOLATE SULFOTRANSFERASE 18 (SOT17) and SOT18 to produce methyl thioalkyl GSL compounds. In the last "side-chain modification" phase, methyl thioalkyl GSLs are catalyzed by a series of enzymatic activities such as oxidation,

Received January 18, 2024. Accepted April 28, 2024.

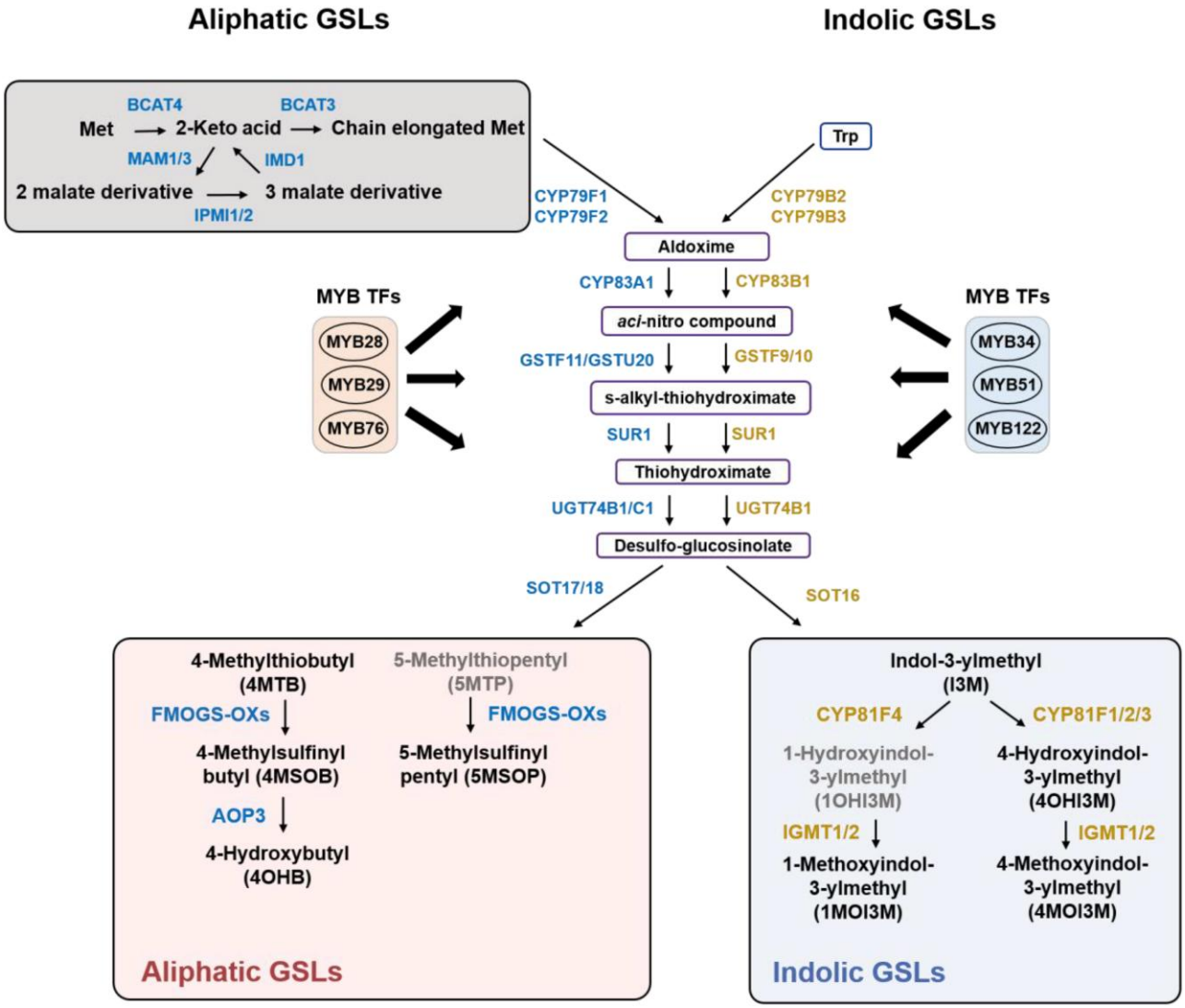

Figure 1. The schematic diagram showing aliphatic and indolic GSL biosynthesis pathways in *Arabidopsis* plants. Production of aliphatic and indolic GSL compounds generally requires 3 and 2 biosynthetic phases, respectively. The green box indicates the first phase, "side-chain elongation" for aliphatic GSL biosynthetic pathway. Aldoxime generated from the "side-chain elongation" phase undergoes the second phase, "core structure formation" to generate DS-GSLs. DS-GSLs enter third phase, "secondary modification" which is indicated with the pink box. DS-GSLs are diversely modified for the production of a variety of aliphatic GSL compounds such as 4OHB, 4MSOB, and 5MSOP. In the case of indolic GSL biosynthesis, Trp enters the "core structure formation" phase to generate DS-GSLs. Next, DS-GSLs undergoes "secondary modification" phase to generate diverse indolic GSL compounds such as 1MOI3M and 4MOI3M. The blue box indicates "the secondary modification" phase of indolic GSL biosynthetic pathway. In both pink and blue boxes, compounds shown with bold dark letters indicate the detected GSL compounds in our HPLC system. In our study using early seedling plants of *Arabidopsis*, 4OHB, 4MSOB, 5MSOP, and 4MTB were detected as major aliphatic GSL compounds. In the case of indolic GSL compounds, I3M, 4OHI3M, 4MOI3M, and 1MOI3M were detected as major indolic GSL compounds. A handful of MYB TFs such as MYB28, MYB29, and MYB76 were shown to control expression of biosynthetic pathway genes related to aliphatic GSL production. Meanwhile, other MYB factors such as MYB34, MYB51, and MYB122 were reported to control expression of biosynthetic genes related to indolic GSL production. The blue and yellow letters indicate the enzymes responsible for the conversion of the aliphatic and indolic compounds, respectively.

alkylation, methoxylation, and desaturation to produce diverse final GSL compounds (Rask et al. 2000; Mikkelsen et al. 2002; Grubb and Abel 2006). For instance, the aliphatic pathway contains several flavin monooxygenases (FMOGS-OXs) that catalyze the conversion of methyl thioalkyl GSLs (i.e. 4-methylthiobutyl, 4MTB) to methylsulfinylalkyl GSLs (i.e. 4-methylsulfinylbutyl, 4MSOB). Methylsulfinylalkyl GSLs are converted into alkenylhydroxalkyl GSLs by 2-oxoglutarate-dependent dioxygenases (i.e. AOP3) (Hansen et al. 2008).

The biosynthesis of indolic GSL compounds begins with the conversion of tryptophan to indole-3-acetaldoxime by CYP79B2/CYP79B3 enzymes. Then, indole-3-acetaldoxime is further catalyzed by a series of catalytic enzymes such as CYP83B1, GSTF9, GSTF10, GGP1, and SUR1 for sulfur incorporation and thiohydroximate formation. Similar to the aliphatic GSL pathway, UGT74B1 catalyzes the glucosylation of thiohydroximate, which is further sulfated by SOT16 to produce indol-3-ylmethyl (I3M) GSL compounds. In the final "side-chain modification" phase, I3M GSLs are catalyzed by various enzymes, as in the aliphatic GSL pathway. In the indolic GS pathway, I3M is hydroxylated by CYP81F enzymes. CYP81F1 to F3 and CYP81F4 are thought to catalyze the production of 4-hydroxyindolic GSL (4OHI3M) and 1-hydroxyindol-3-ylmethyl (1OHI3M), respectively (Pfalz et al. 2011). These compounds are further methylated by INDOLE

GLUCOSINOLATE METHYLTRANSFERASE 1 (IGMT1) and IGMT2 to produce 1-methoxy-indol-3-ylmethyl (1MOI3M) and 4-methoxy-indol-3-ylmethyl (4MOI3M), respectively.

Several R2R3-type MYB transcription factors (TFs) regulate GSL biosynthesis. MYB28, MYB29, and MYB76 regulate the production of aliphatic GSLs (Hirai et al. 2007; Sonderby et al. 2007; Gigolashvili et al. 2008). The *myb28myb29* double mutant of *MYB28* and *MYB29* was almost completely deficient in aliphatic GSLs, and overexpression of *MYB28*, *MYB29*, and *MYB76* elevated the number of aliphatic GSLs (but not indolic GSLs) via the upregulated expression of aliphatic GSL pathway genes. Unexpectedly, gene expression in the indolic GSL pathway was reduced, suggesting a regulatory balance between aliphatic and indolic GSL levels (Gigolashvili et al. 2007; Sonderby et al. 2010). Three other MYB TFs—MYB34, MYB51, and MYB122—are also involved in the production of indolic GSL compounds (Celenza et al. 2005; Gigolashvili et al. 2007; Malitsky et al. 2008). Analysis of the triple mutant *myb34myb51myb122* showed almost no detectable indolic GSLs, indicating that these 3 MYB TFs are essential activators for indolic GSL production.

A close link between light and GSL metabolism has been reported. Exposure to light increases total GSL content in plants, thus exhibiting diurnal fluctuation with an increase during the daytime and a decrease at night. In addition, long-term darkness results in a substantial reduction in the amount of endogenous GSLs (Huseby et al. 2013). Two enzymatic genes involved in the early side-chain elongation of aliphatic GSLs, *BCAT4* and *MAM1*, display higher transcript levels under light conditions than under dark conditions (Schuster et al. 2006). The sulfotransferase gene *SOT17* in the aliphatic GSL pathway also exhibits higher transcript levels under light conditions and reduced levels in the dark (Klein et al. 2006). Furthermore, the expression of AOP2 in the aliphatic GSL pathway is higher under continuous light than under continuous darkness (Neal et al. 2010).

In addition to GSL metabolism, a close link between light and sulfate assimilation has been reported (Koprivova and Kopriva 2014). One of the key genes for sulfate assimilation, *ADENOSINE 5′-PHOSPHOSULFATE REDUCTASE*, (*APR*), displays diurnal rhythm in *Arabidopsis* and maize, with a peak during daylight hours. The enzymatic activity of APR is reduced under dark conditions and increased upon exposure to light. A bZIP TF, ELONGATED HYPOCOTYL 5 (HY5), has been shown to directly bind to and regulate the expression of *APR* under light conditions (Lee et al. 2011).

GSLs are produced in Brassicaceae plants such as oilseed rape (*Brassica napus* L.), cabbage (*Brassica oleracea* L. var. *capitata*), broccoli (*B. oleracea* var. *italica*), Chinese cabbage (*Brassica rapa* L. var. *pekinensis*), and the model plant *A. thaliana* (Fahey et al. 2001; Barillari et al. 2005). Over 137 different GSL structures have been proposed for various members of the Brassicaceae family (Blazevic et al. 2020). As in other families, light signaling is closely related to GSL metabolism in Brassicaceae plants. However, the molecular mechanisms underlying the light-mediated regulation of GSL metabolism are not well understood.

Therefore, in the present study, we aimed to elucidate the mechanisms relating to light signaling and GSL biosynthesis. Because HY5 is one of the key players in light signaling, the possible role of HY5 in controlling GSL metabolism was investigated. In this study, we found that HY5 suppressed GSL accumulation of GSLs via suppressing GSL pathway genes. HY5 interacts with histone deacetylases (HDAs) to modulate the epigenetic context of GSL metabolic genes. This study provides evidence that HY5 is involved in the epigenetic modulation of GSL accumulation in *Arabidopsis*.

Results

GSL contents in *Arabidopsis* seedlings under light and dark conditions

Endogenous amounts of aliphatic and indolic GSLs were measured in whole *Arabidopsis* plants grown under 1 wk of long-day (LD) (16-h light and 8-h dark) or continuous dark conditions. For the light condition samples, seedlings were harvested 4 h after light irradiation (ZT4) on the final day. For the dark condition samples, seedlings were harvested in the dark. Based on the ultra-high-performance liquid chromatography (UHPLC) and LC/MS analysis results, we identified 4 major aliphatic GSLs, 4-hydroxybutyl (4OHB), 4MSOB, 5-methylsulfinylpentyl (5MSOP), and 4MTB; 4 indolic GSLs, I3M, 4OHI3M, 4MOI3M, and 1MOI3M; and 1 aromatic GSL, 2-phenylethyl (Supplementary Fig. S1 and Table S1). Because only 1 aromatic GSL was detected, it was excluded, and further analyses focused only on aliphatic and indolic GSL compounds. Among the 4 aliphatic GSLs, 4MTB was the most dominantly detected, followed by 4MSOB and 4OHB, and then 5MSOP, with low levels under both light and dark conditions (Fig. 2A). Among the 4 indolic GSLs, 1MOI3M was the most abundant, followed by I3M, and then by 4OHI3M and 4MOI3M (Fig. 2B). The total amounts of aliphatic (1,202 nmol/g) and indolic (392 nmol/g) GSLs under light conditions were 3.0 times higher than those under dark conditions (322 nmol/g) (Fig. 2C and Supplementary Table S2). Taken together, these data indicate that light stimulates the biosynthesis of both aliphatic and indolic GSLs in young *Arabidopsis* seedlings.

Next, we assessed the completion of the "side-chain modification" phase of the aliphatic pathway, which synthesizes 4MTB (highlighted with the pink box in Fig. 1). 4MTB (801 nmol/g under light conditions) was highly detected (Supplementary Table S2), whereas other compounds, such as 5MTP, were not (gray letters in Fig. 1). This suggests that other substrates (i.e. 5MTP) were immediately converted into 4MTB. 4MSOB and 4OHB, which are produced from 4MTB (Fig. 1), were also abundantly detected among the aliphatic GSLs in both light and dark samples (Fig. 2A; Supplementary Fig. S1 and Table S2). This indicates that the 4MTB–4MSOB–4OHB production pathway occurred prominently in *Arabidopsis* seedlings.

To assess the indolic GSL pathway, we analyzed the amounts of indolic GSLs and observed that 1MOI3M was more abundantly detected than 4OHI3M or 4MOI3M (Fig. 2B). Since CYP81F4 mainly converts I3M to 1OHI3M, the precursor for 1MOI3M, whereas CYP81F1 to F3 convert I3M to 4OHI3M, the precursor for 4MOI3M (Pfalz et al. 2011) (Fig. 1), this observation suggested that CYP81F4 played a greater role than CYP81F1 to F3 in the *Arabidopsis* seedlings. We could not detect 1OHI3M, suggesting its rapid conversion to 1MOI3M by CYP81F4. To test this hypothesis, we quantified the expression of *CYP81F1* to *F4* in the seedlings and found that *CYP81F4* showed the most robust expression among CYP81F1 to F4 genes (Supplementary Fig. S2). Thus, it is likely that the I3M–1MOI3M production pathway was dominant over the I3M–4MOI3M in the *Arabidopsis* seedlings. Collectively, the total amount of GSLs was higher under light than under dark conditions (Fig. 2C). In addition, the amount of aliphatic GSLs was significantly higher than that of indolic GSLs under both light and dark conditions.

Diurnal variation in GSL levels in *Arabidopsis* seedlings

It has been previously reported that the GSL content fluctuates throughout the day, exhibiting a diurnal rhythm (Huseby et al. 2013).

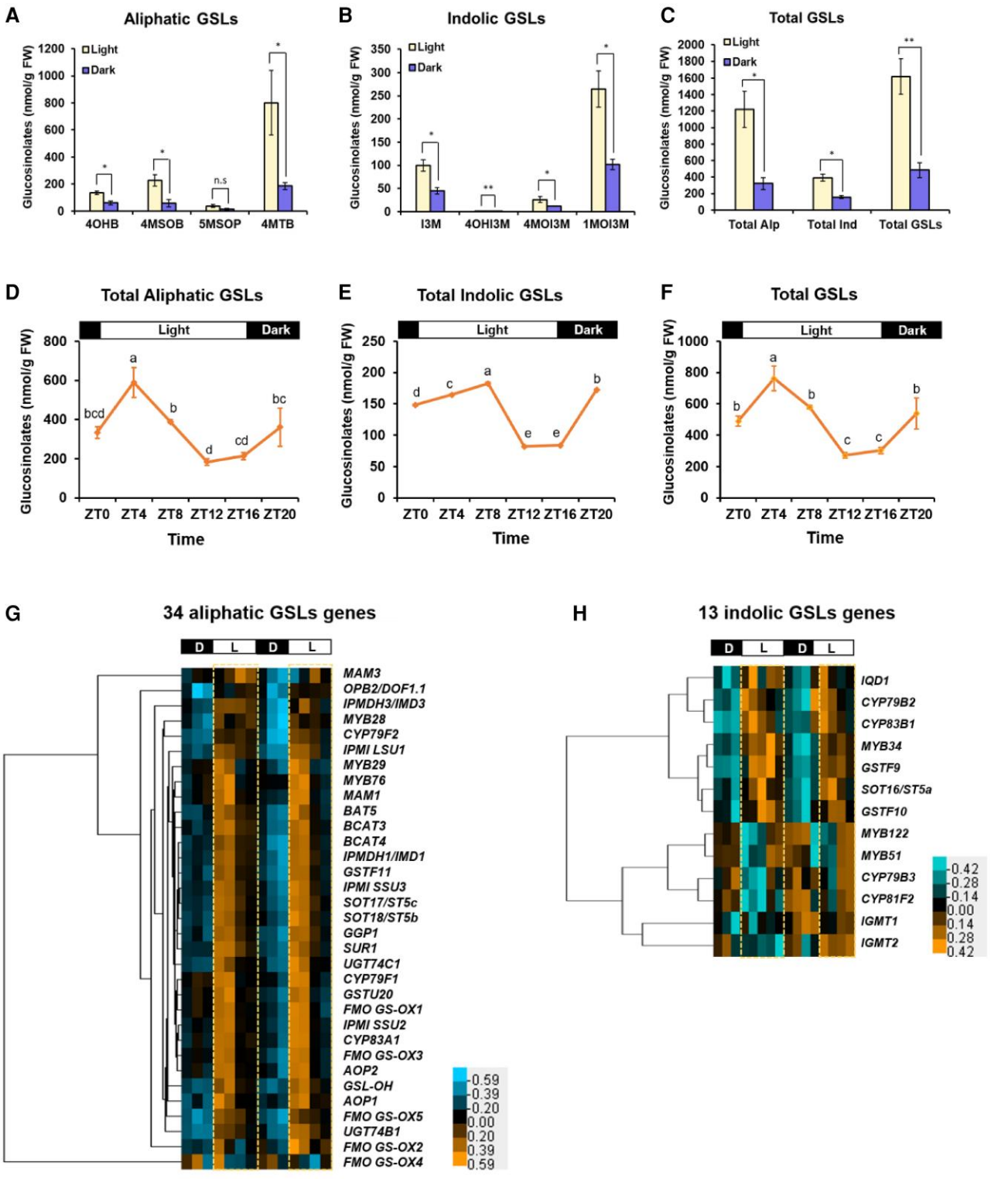

Figure 2. GSL contents in *Arabidopsis* seedlings under light and dark conditions. The composition and content of aliphatic GSLs **(A)**, indolic GSLs **(B)**, and total GSLs **(C)**. One-wk-old Col-0 seedlings grown under either a LD condition (16-h light and 8-h dark) or a continuous dark condition. Biological triplicates ($n = 3$) were statistically analyzed by Student's *t*-test (n.s., not significant; $^{*}P \leq 0.05$; $^{**}P \leq 0.01$). **A to C)**. 4OHB, 4MSOB, 5MSOP, 4MTB, I3M, 4OHI3M, 4MOI3M, 1MOI3M, Total Alp, total aliphatic GSL; Total Ind, total indolic GSL. Contents of aliphatic GSLs **(D)**, indolic GSLs **(E)**, and total GSLs **(F)** contents under a LD condition. One-wk-old seedlings were harvested at the indicated zeitgeber time (ZT) points for GSLs extraction. Each result represents the mean ± SD of 3 independent biological replicates ($n = 3$) per treatment. Different letters represent significant differences ($P < 0.05$) determined by one-way ANOVA with Tukey's post hoc test. Heatmap of 34 aliphatic GSL pathway genes **(G)** or 13 indolic GSL pathway genes **(H)** along time points in a day. D, dark; L, light.

To confirm this, we harvested 1-wk-old *Arabidopsis* seedlings at 4 h intervals to measure the GSL content. The total amount of aliphatic GSLs increased significantly from ZT0 to ZT4 and steadily decreased until ZT12 before increasing slightly until ZT20 (Fig. 2D). The total indolic GSL content also exhibited a diurnal rhythm, moderately increasing from ZT0 to ZT8, decreasing rapidly from ZT12 to ZT16, and then drastically increasing until ZT20 (Fig. 2E). The pattern of total GSLs was similar to that of aliphatic GSLs, with a peak at ZT4 and a gradual decrease thereafter, showing the lowest level at ZT12 and then increasing to ZT20 (Fig. 2F). These data indicate that the endogenous production of total GSLs undergoes a diurnal rhythm, with high levels during the day and low levels at night.

Daytime expression of GSL biosynthesis genes

To confirm the daytime abundance of GSLs, we analyzed the expression patterns of 34 aliphatic and 13 indolic GSL pathway genes along the diurnal time course, which were obtained from a previous study (Jung et al. 2016). Most aliphatic GSL pathway genes showed higher expression during the day and were significantly downregulated at night (Fig. 2G). Indolic GSL pathway genes displayed a more complicated pattern than the aliphatic GSL pathway genes during the light/dark cycle (Fig. 2H). Altogether, these data indicate that GSL compounds, particularly aliphatic GSL compounds, are highly synthesized via the active expression of biosynthetic genes in the morning.

GSL contents in *hy5* mutants

HY5 is a key player in light-mediated morphogenesis in *Arabidopsis* and is involved in sulfate assimilation, which is closely related to GSL biosynthesis because GSL metabolism requires sulfur. Furthermore, the expression of several GSL pathway genes was affected in *hy5* mutants in a past study (Huseby et al. 2013). Therefore, we tested whether HY5 is involved in the GSL biosynthetic pathway under light conditions by measuring GSL levels in Columbia-0 (Col-0) wild-type (WT) plants and *hy5-215* mutants after harvesting seedlings at 4-h intervals (Fig. 3). The amount of total aliphatic GSLs was significantly higher in *hy5-215* mutants than in Col-0 plants, except at ZT20 (Fig. 3A). All individual aliphatic GSL compounds (4MTB, 4MSOB, 4OHB, and 5MSOP) exhibited increased levels in mutants compared with those in Col-0 in tested time points (Supplementary Fig. S3). In contrast, indolic GSLs were lower in *hy5-215* mutants than in Col-0, except at ZT12 (Fig. 3B). This implies that the effect of HY5 may be more complex than that of aliphatic GSLs under light conditions. Therefore, the role of HY5 in the biosynthesis of indolic GSL requires further investigation.

By virtue of aliphatic GSLs, the total amount of GSLs was significantly higher in *hy5-215* mutants than in Col-0 plants, except at ZT4 and ZT20 (Fig. 3C). These data indicate that HY5 plays a repressive role in aliphatic GSL biosynthesis and a more complex role in indolic GSL biosynthesis in *Arabidopsis* seedlings.

Because the *hy5-215* mutant exhibited increased levels of aliphatic GSL compounds, we compared aliphatic GSL compounds in *35S::HY5-GFP/hy5-215* transgenic plants, Col-0 controls, and *hy5-215* mutants (Supplementary Fig. S4). The amounts of total GSLs were elevated in *hy5-215* mutants and substantially restored in *35S::HY5-GFP/hy5-215* plants to levels comparable to those in Col-0 plants (Supplementary Fig. S4C). All 4 aliphatic GSLs (4OHB, 4MSOB, 5MSOP, and 4MTB) that showed higher levels in *hy5-215* mutants were significantly repressed in *35S::HY5-GFP/hy5-215* plants, with comparable levels to those in Col-0 plants (Supplementary Fig. S4A). This indicates that HY5 plays a negative role in aliphatic GSL biosynthesis in *Arabidopsis*. In the case of indolic GSLs, 1MOI3M and 4OHI3M were suppressed in *35S:HY5-GFP/hy5-215* transgenic plants, with higher levels observed in the *hy5-215* mutants than in Col-0 plants (Supplementary Fig. S4B). However, I3M and 4MOI3M levels were not different between *35S::HY5-GFP/hy5-215* transgenic plants and Col-0 plants, suggesting a more complex involvement of HY5 in indolic GSL biosynthesis in *Arabidopsis* seedlings.

RNA sequencing analysis of Col-0 and *hy5-215* mutants

As *hy5-215* mutants and *35S::HY5-GFP/hy5-215* transgenic plants showed opposite GSL content profiles, particularly regarding aliphatic GSL compounds, the expression profile of GSL pathway genes was determined by RNA sequencing (RNA-seq) and compared between Col-0 and *hy5-215* plants. Association heatmap analysis confirmed close grouping between samples, indicating that RNA-seq library construction was successful (Supplementary Fig. S5A). After trimming the low-quality reads, all cleaned reads were mapped to over 97% of the *Arabidopsis* reference genome TAIR 10 using Tophat2 with default parameters (Kim et al. 2013) (Supplementary Table S3). Using the edgeR package, 862 genes were identified as differentially expressed (differentially expressed genes, DEGs) between Col-0 plants and *hy5-215* mutants (Fig. 4A and Supplementary Fig. S5B). Gene ontology (GO) analysis using 862 DEGs (460 and 402 up- and downregulated, respectively, in *hy5-215* vs Col-0) listed GSL biosynthetic process as the top category (Fig. 4B, indicated with a red color bar). Heatmap analysis and the Venn diagram analysis of the DEGs overlapped with 47 GSL metabolic genes obtained from TAIR (https://www.arabidopsis.org) showed that 12 GSL pathway genes were upregulated in *hy5-215* mutants (Fig. 4, C and D). However, no GSL pathway genes were identified in the downregulated DEGs (Supplementary Fig. S5C). Among the 12 upregulated genes, 11 aliphatic GSL pathway genes (*MYB29*, *CYP79F1*, *CYP79F2*, *CYP83A1*, *BCAT4*, *BAT5*, *MAM1*, *IMD1*, *IPMI2*, *FMOGS-OX1*, and *FMOGS-OX3*) and 1 indolic GSL pathway gene (*CYP81F2*) were identified (Fig. 4, C and D). These data indicated that HY5 suppressed GSL metabolic genes in *Arabidopsis*.

To verify the RNA-seq results, the transcript levels of GSL pathway genes in Col-0, *hy5-215* mutant, and *35S::HY5-GFP/hy5-215* transgenic plants were quantified by reverse-transcription quantitative polymerase chain reaction (RT-qPCR) analysis (Fig. 5). First, we measured the transcript levels of aliphatic pathway genes, including 1 MYB TF gene (*MYB29*), 5 genes in the side-chain elongation phase (*BCAT4*, *BAT5*, *IMD1*, *IPMI*, *SSU2*, and *MAM1*), 3 genes in the core structure formation phase (*CYP79F1*, *CPY79F2*, and *CYP83A1*), and 2 genes in the secondary modification phase (*FMOGS-OX1* and *FMOGS-OX3*). All 11 aliphatic GSL pathway genes were significantly upregulated in *hy5-215* mutants compared to levels in Col-0 plants but were fully suppressed in *35S::HY5-GFP/hy5-215* transgenic plants (Fig. 5A). Consistent with the RNA-seq data, *CYP81F2* expression was significantly upregulated in *hy5-215* mutants and restored to Col-0 levels in *35S::HY5-GFP/hy5-215* transgenic plants (Supplementary Fig. S6). Unexpectedly, many of the tested indolic GSL pathway genes were considerably repressed in *35S::HY5-GFP/hy5-215* transgenic plants, implying that HY5 might function as a repressor of indolic GSL pathway genes. Taken together, these data indicate that HY5 represses GSL biosynthetic processes, particularly aliphatic GSL, via the transcriptional suppression of GSL pathway genes under light conditions.

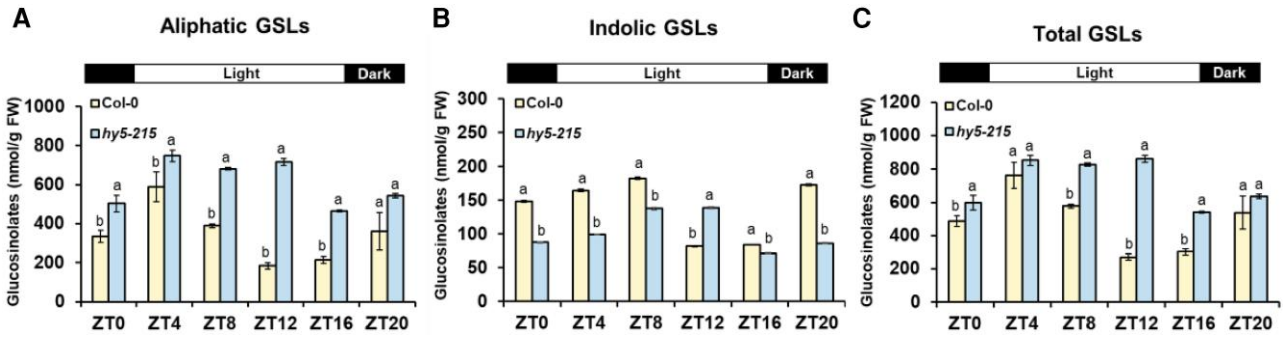

Figure 3. GSL contents in Col-0 plants and *hy5-215* mutants under a LD condition. Comparison of aliphatic GSL **(A)**, indolic GSL **(B)**, and total GSL **(C)** contents. One-wk-old seedlings were harvested every 4 h starting from ZT0 time point. Each result represents the mean ± SD of 3 independent biological replicates ($n = 3$). Different letters represent significant differences ($P < 0.05$) determined by one-way ANOVA with Tukey's post hoc test.

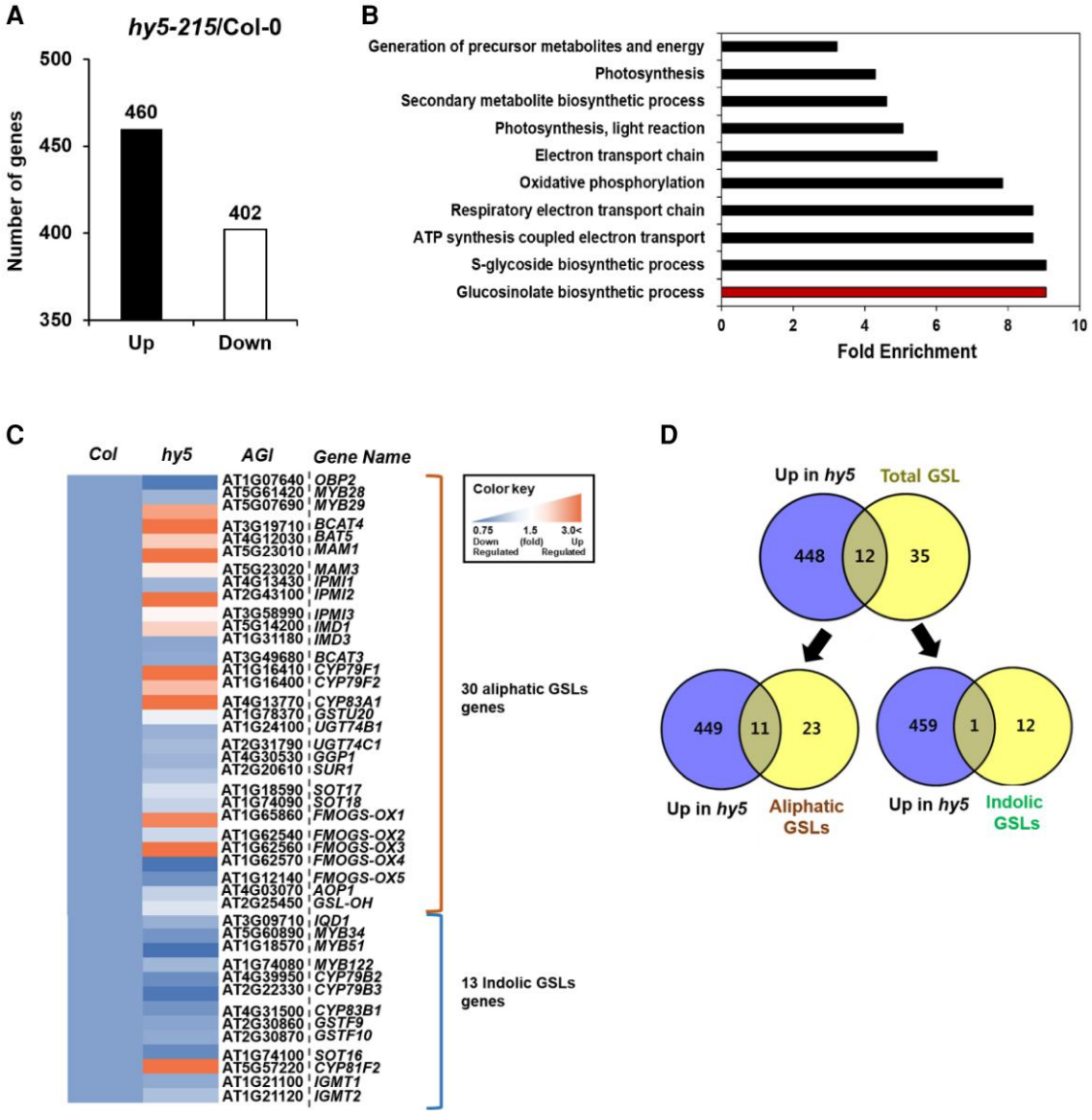

Figure 4. Identification of DEGs between Col-0 and *hy5-215* plants. One-wk-old seedlings grown under a LD condition were harvested at ZT4 for transcriptome analysis. Biological triplicates were analyzed. **A)** The number of DEGs identified by pair-wise comparison analysis between Col-0 and *hy5-215*. **B)** GO analysis of 460 upregulated genes in *hy5-215* when compared to levels of Col-0. Top 10 GO terms were detected using ShinyGO (ver0.77) webtool. The first ranked GO term "glucosinolate biosynthetic process" is indicated with a red bar. **C)** Heatmap of 30 aliphatic and 13 indolic GSL pathway genes between Col-0 and *hy5-215* mutant. Each block of value represents the mean of 3 replicates. The mean value of Col-0 was normalized to 1. **D)** Venn diagram between 460 upregulated genes and 47 GSL pathway genes.

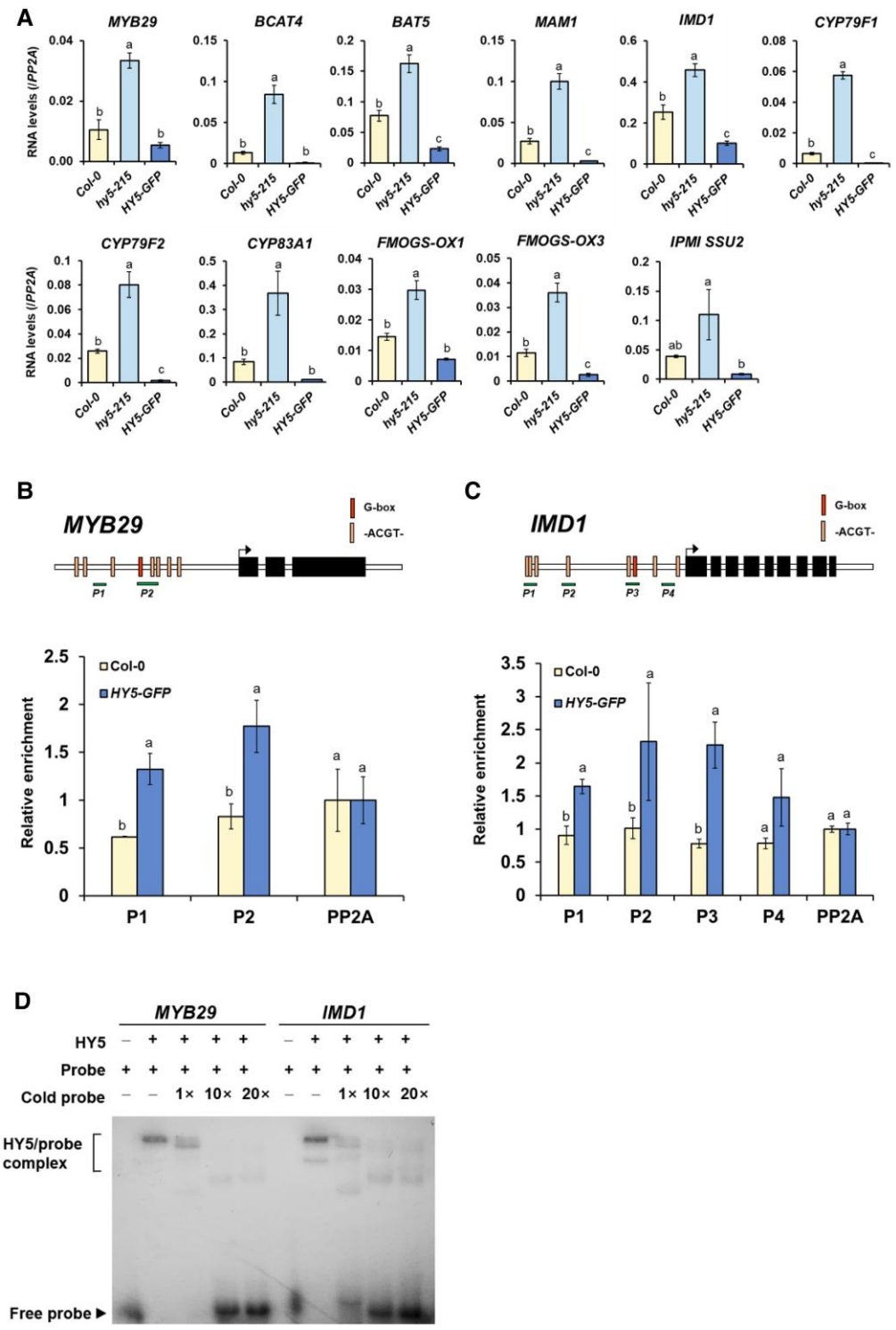

Figure 5. HY5 directly controls the expression of *MYB29* and *IMD1*. **A)** Results of RT-qPCR analysis of 11 aliphatic GSL pathway genes in Col-0 WT, *hy5-215* mutant, and 35S::*HY5-GFP*/*hy5-215* transgenic lines. One-wk-old seedlings grown under a LD condition were harvested at ZT4 for RNA extraction. Each result represents the mean ± SD of 3 independent biological replicates ($n = 3$). Different letters represent significant differences ($P < 0.05$) determined by one-way ANOVA with Tukey's post hoc test. Results of ChIP-qPCR for genomic region of *MYB29* **(B)** and *IMD1* **(C)** using 35S::*HY5-GFP*/*hy5-215* transgenic lines. One-wk-old seedlings were crosslinked at ZT4. Upper panel: Schematic diagram indicating the amplicons within promoter region used in the ChIP-qPCR assay. The amplicon-amplifying gene body region of reference gene *PP2A* (AT1G69960) was used as a control. Bottom panel: Result of ChIP-qPCR. Precipitated and input DNA from ChIP assay using antibody against GFP was used for qPCR, and then, the relative enrichment was determined by comparing to the values of *PP2A* (set as 1). Each result represents the mean ± SD of 3 independent biological replicates ($n = 3$). Different letters represent significant differences ($P < 0.05$) determined by one-way ANOVA with Tukey's post hoc test. **D)** Result of EMSA using recombinant HY5 protein. The 80-bp promoter fragments containing the G-box sequence were prepared as probes. Total 1 pmol of each ^{32}P-labeled probe was incubated with 2 μg of HY5 for 30 min. Cold competitor probes were generated from dimerized oligos without labeling.

Suppression of *MYB29* and *IMD1* by HY5

It has been reported that the bZIP domain protein HY5 binds to ACGT-containing elements (ACEs), especially the G-box motif (-CACGTG-), in *Arabidopsis* plants (Burko et al. 2020). To identify the direct targets of HY5, we first analyzed whether the 12 DEGs in the GSL pathway possessed ACEs, including G-box motifs. All 12 genes contained at least 1 ACE in their promoter regions (Supplementary Fig. S7). We performed chromatin immunoprecipitation (ChIP) followed by real-time quantitative PCR analysis (ChIP-qPCR) of these candidate genomic regions. HY5 primarily bound to the promoter region of *MYB29* in the aliphatic GSL pathway (Fig. 5B). The promoter region of *MYB29* contained 1 G-box (-GAGCTC-) and 7 ACEs (-ACGT-). Promoter regions (P1 and P2) containing a G-box exhibited a significant enrichment of HY5-GFP compared to Col-0 plants, as did the internal negative reference gene, *PP2A* (AT1G69960). This suggests that the G-box in the promoter of *MYP29* might mediate the recruitment of HY5 in *Arabidopsis* plants. Among GSL metabolic genes, HY5 was shown to substantially bind to *IMD1*, which is a gene involved in the "chain elongation" process of aliphatic GSL biosynthesis (Fig. 5C). The promoter region of *IMD1*, containing 1 G-box motif and 7 ACE motifs, was broadly and highly enriched with HY5-GFP in comparison with Col-0 plants, as was the internal negative reference gene *PP2A*. Electrophoretic mobility shift assay (EMSA) analysis using recombinant HY5 protein showed that the HY5 binds to the G-box motif of the promoters of *MYB29* and *IMD1* (Fig. 5D). Taken together, these results indicate that HY5 regulates aliphatic GSL metabolism by directly targeting *MYB29* and *IMD1* under light conditions.

Role of HY5 and HISTONE DEACETYLASE9 in the regulation of GSL metabolism

As HY5 plays a negative role in the transcription of MYB TFs and GSL pathway genes, we postulated that it might work alongside repressive histone modifiers such as HDAs or histone methyltransferases [i.e. POLYCOMB REPRESSIVE COMPLEXES 2 (PRC2) and PRC1 complexes]. To test this hypothesis, we performed yeast two-hybrid assays between HY5 and histone modifiers, including 14 HDAs and 5 components of the PRC2 and PRC1 complexes (Supplementary Fig. S8, A and B). HY5 was shown to interact with several HDAs, but not with components of the PRC2 and PRC1 complexes (Supplementary Fig. S8, A and B). HISTONE DEACETYLASE9 (HDA9) showed the strongest interaction with HY5 (Supplementary Fig. S8C). We further confirmed that HY5 interacted with HDA9 using an in vitro pull-down assay and a split-luciferase complementation imaging (LCI) assay (Supplementary Fig. S8, D and E).

Next, we investigated whether HDA9 was involved in the regulation of GSL metabolism. HPLC analysis of the Col-0 and *hda9-1* mutants was performed to measure the total GSL content (Fig. 6A). Aliphatic and indolic GSL contents were significantly higher in the *hda9-1* mutants, particularly during daytime, than in Col-0 plants (Fig. 6, B and C). We also performed RT-qPCR analysis of Col-0 and *hda9-1* mutants. Consistent with the HPLC data, all 11 aliphatic GSL pathway genes were significantly upregulated in *hda9-1* mutant compared to levels in Col-0 plants (Fig. 6D). Taken together, these data indicate that HY5 associates with HDA9 to coordinate the transcriptional suppression of GSL pathway genes in *Arabidopsis* plants.

Role of HY5 in the HDA9-mediated H3 deacetylation of GSL target genes

We performed a ChIP assay using 2 independent *HDA9-FLAG/hda9-1* complemented transgenic lines (#4–6 and #6–5) to determine whether HDA9 also targets *MYB29* and *IMD1*, 2 HY5 target genes involved in GSL metabolism. The ChIP-qPCR results showed that the promoter regions of *MYB29* and *IMD1* were substantially enriched with HDA9-FLAG (Fig. 7, A and B). This suggests that HY5 and HDA9 cooperate to regulate GSL metabolism, particularly via direct regulation of *MYB29* and *IMD1* in the GSL pathway.

Previous studies reported that HDA9 deacetylates H3K9ac and H3K27ac on target chromatin (Chen et al. 2016; Zheng et al. 2016). Since HY5 physically associates with HDA9, we tested whether HY5 is required for the histone deacetylase activity of HDA9 on target GSL genes by performing a ChIP assay using H3K9ac and H3K27ac antibodies to compare the level of H3 acetylation between Col-0 and *hy5-215* mutants. The level of H3K9ac acetylation was substantially higher in the genomic regions of *MYB29* and *IMD1* in *hy5-215* mutants than in Col-0 plants (Fig. 7, C and D), indicating that HY5 is required for HDA9-dependent de-acetylation to suppress GSL biosynthesis. Meanwhile, we did not detect a significant difference in H3K27ac levels in the *MYB29* and *IMD1* regions between Col-0 and *hy5-215* plants (Supplementary Fig. S9).

To further confirm whether *MYB29* and *IMD1* genes are directly repressed by HY5 via HDA9, we conducted RT-qPCR analysis to quantify transcript levels of *MYB29* and *IMD1* between Col-0, *hy5-215*, *hda9-1*, and *hy5-215; hda9-1* double mutant. As a result, HDA9 was shown to be epistatic to HY5 in the regulation of *MYB29* and *IMD1* (Fig. 7, E and F). These results confirmed that *MYB29* and *IMD1* are under the direct suppression of HY5 via HDA9 in *Arabidopsis*.

In summary, we found that in an *Arabidopsis* model plants, HY5 acts to reduce the production of endogenous GSL via transcriptional suppression of GSL biosynthetic genes, particularly aliphatic GSL pathway genes, during the daytime. HY5 acts together with HDA9 to suppress the GSL pathway genes via histone H3K9 deacetylation. Therefore, we conclude that the HY5–HDA9 module plays an important role in the daily modulation of the GSL profile, perhaps to properly optimize daily metabolism.

Discussion

In this study, we found that HY5 is involved in the modulation of endogenous GSL production during the daytime by controlling the expression of MYB TF and GSL metabolic genes.

Among the aliphatic and indolic GSLs, the total amount of aliphatic GSLs was higher than that of indolic GSLs under both light and dark conditions (Fig. 2C). This suggests that aliphatic GSLs play a more defensive role than indolic GSLs in young *Arabidopsis* seedlings grown under light conditions. In addition, both aliphatic and indolic GSLs were actively synthesized under early (ZT0–ZT8) and LD light conditions, with the highest peaks at ZT4 (aliphatic GSLs) and ZT8 (indolic GSLs) under light conditions (Fig. 2, D and E). High levels of aliphatic GSL compounds were attributed to the biosynthetic process in the 4MTB–4MSOB–4OHB production pathway (Fig. 2A). A sequential enzymatic process involving *ST5B–C*, *FMO GS-OXs*, and *AOPs* may be responsible for this pathway (Fig. 1). These metabolic genes exist as multiple homologs in the *Arabidopsis* genome; however, their individual metabolic roles have not yet been clearly defined. Thus, to determine which genes

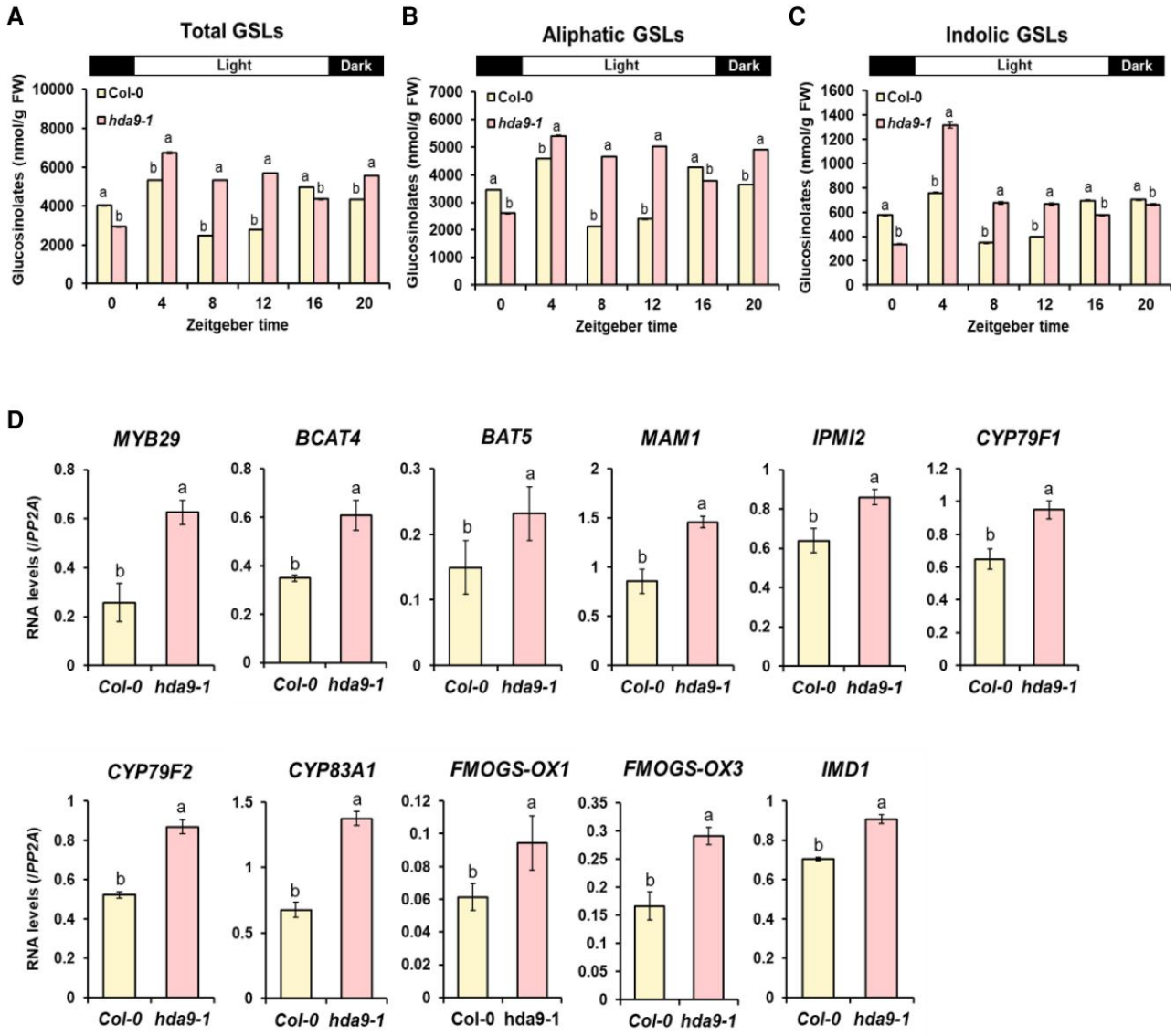

Figure 6. GSL contents under a LD condition in Col-0 and *hda9-1* plants. Comparison of total GSL **(A)**, aliphatic GSL **(B)**, and indolic GSL **(C)** contents. One-wk-old seedlings were harvested every 4 h starting from ZT0 time point. **D)** Results of RT-qPCR analysis of 11 aliphatic GSL pathway genes between Col-0 and *hda9-1* mutant. One-wk-old seedlings grown under a LD condition were harvested at ZT4 for RNA extraction. **A to D)** Each result represents the mean ± SD of 3 independent biological replicates ($n = 3$). Different letters represent significant differences ($P < 0.05$) determined by one-way ANOVA with Tukey's post hoc test.

play a major role in the 4MTB–4MSOB–4OHB biosynthesis pathway, their expression levels over a diurnal time course were collected and compared (Supplementary Fig. S10). Transcripts of most of the secondary modification phase genes exhibited the highest peak at ZT4 and decreased later in the day, similar to the highest amount of GSLs in the day. Expression of *AOP3* was not detected in the dataset, implying that *AOP3* was not expressed in the tested young seedlings.

In the "secondary modification" phase of the aliphatic GSL pathway, Col-0 was detected to have 1 dominant methyl thioalkyl GSL, 4MTB, (Figs. 1 and 2A). 4MTB can be converted into 4MSOB by the enzymatic activity of FMOGS-OXs and subsequently converted into 4OHB or 3-butenyl by the dioxygenase activities of AOP3 or AOP2, respectively (Fig. 1). Although 4MSOB can be used as a substrate for conversion to 3-butenyl by the dioxygenase activity of AOP2, 3-butenyl was not detected in *Arabidopsis* early seedlings. This phenomenon may be explained by the fact that the *Arabidopsis* Col-0 ecotype possesses a null allele of *AOP2* because of a 5-bp deletion at base 484, resulting in a severely truncated protein (Kliebenstein et al. 2001). Thus, it is likely that AOP1 and AOP3 play a major role in the conversion step of 4MSOB, resulting in 4OHB production instead of 3-butenyl in Col-0 plants. However, as shown in Supplementary Fig. S10, we observed that *AOP3* was merely detected in *Arabidopsis* young seedlings, whereas *AOP1* is strongly expressed, suggesting that AOP1 might play a crucial role in the conversion of 4MSOB to 4OHB. Further experimental confirmation is required.

It was shown that GSLs are highly synthesized in the light condition compared to dark condition (Fig. 2, A to C). We further examined the amounts of GSLs in different photoreceptor mutants such as *phyA-211*, *phyB-9*, and *cry1*; *cry2*. GSLs were increased in these photoreceptor mutants (Supplementary Fig. S11A). However, *phyA-211* mutant exhibited the most increase in GSLs compared to those of Col-0 and other photoreceptor mutants

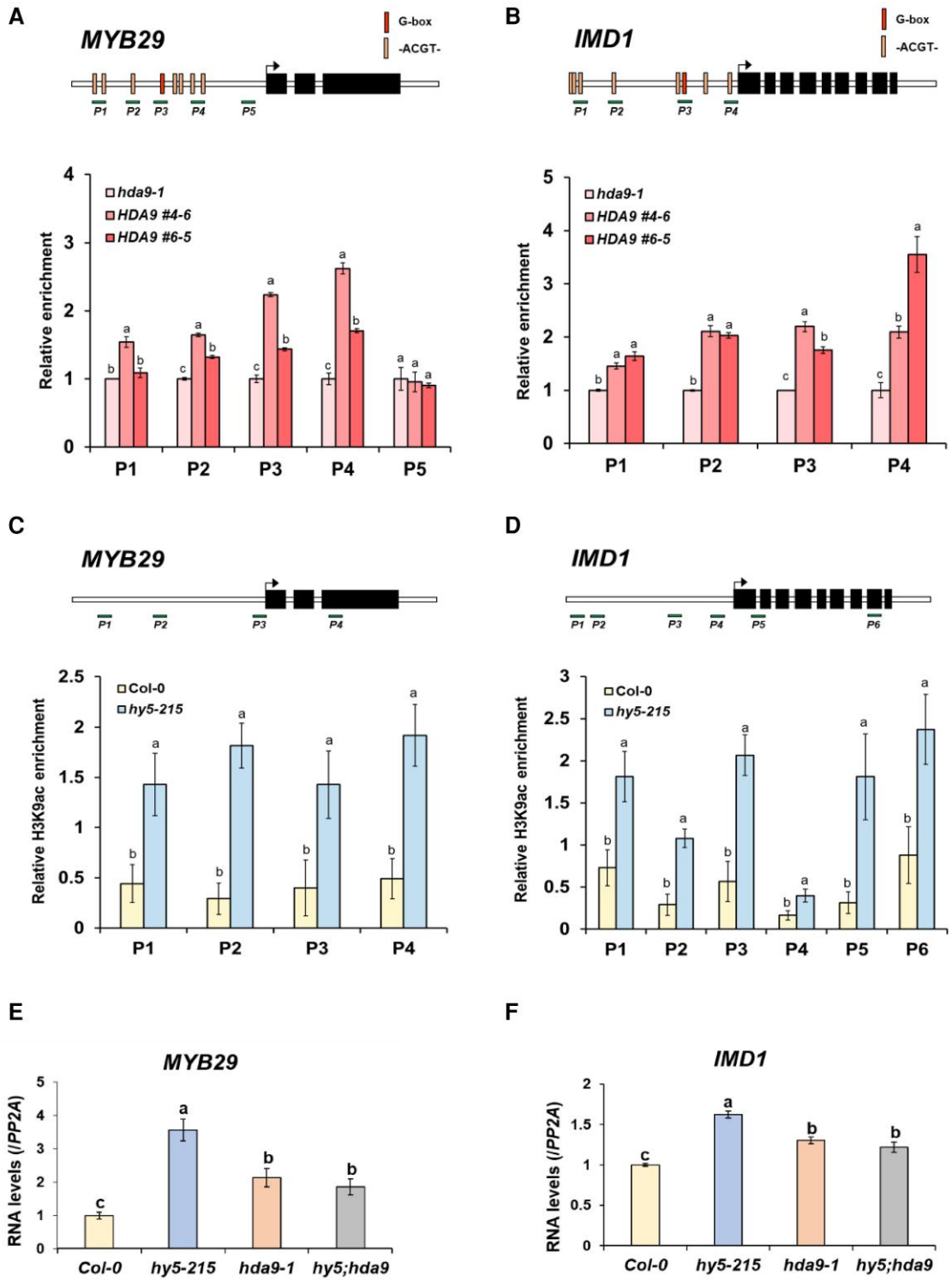

Figure 7. Role of HY5 in HDA9-mediated suppression of *MYB29* and *IMD1*. Results of ChIP-qPCR for genomic region of *MYB29* **(A)** and *IMD1* **(B)** using *HDA9-FLAG/hda9-1* transgenic lines. One-wk-old seedlings were crosslinked at ZT4. Upper panel: Schematic diagram indicating the amplicons within promoter region used in the ChIP-qPCR assay. The amplicon-amplifying gene body region of reference gene *PP2A* (AT1G69960) was used as a control. Bottom panel: Result of ChIP-qPCR. Precipitated and input DNA from ChIP assay using antibody against FLAG epitope was used for qPCR, and then, the relative enrichment was determined by comparing to the values of *PP2A* (set as 1). Enrichment of H3K9ac level on the genomic region of *MYB29* **(C)** and *IMD1* **(D)** between Col-0 and *hy5-215*. Upper panel: Schematic diagram indicating the amplicons within promoter region used in the ChIP-qPCR assay. The amplicon-amplifying gene body region of reference gene *PP2A* (AT1G69960) was used as a control. Bottom panel: Result of ChIP-qPCR. Precipitated and input DNA from ChIP assay using antibody against H3K9ac epitope were used for qPCR. Results of RT-qPCR analysis of *MYB29* **(E)** and *IMD1* **(F)** gene between Col-0, *hy5-215*, *hda9-1*, and *hy5-215*; *hda9-1* double mutant. One-wk-old seedlings grown under a LD condition were harvested at ZT4 for RNA extraction. **A to F)** Each result represents the mean ± SD of 3 independent biological replicates ($n = 3$). Different letters represent significant differences ($P < 0.05$) determined by one-way ANOVA with Tukey's post hoc test.

(Supplementary Fig. S11A). These data suggest that phyA has a major impact on HY5-mediated suppression of GSLs. To a lesser extent, phyB and CRY1/CRY2 also contribute to the HY5-mediated suppression of GSL biosynthesis (Supplementary Fig. S11A). It indicates that light signaling might exert a negative impact on the biosynthesis of GSLs. In addition, we quantified amounts of GSLs under different light conditions (red, far-red, blue, dark, and white light). We noticed that continuous far-red light displayed the most suppressive impact on the biosynthesis of GSLs (Supplementary Fig. S11B). This is consistent with the most increased amounts of GSLs in the *phyA-211* background. These observations led us to conclude that photoreceptor (particularly phyA)-mediated light signaling might play a negative role in the GSLs biosynthesis possibly via HY5.

Regarding the observation (in Fig. 2, A to C) that light increases the amounts of GSLs in comparison to those of dark, it makes sense in terms of the fact that the output of photosynthesis, glucose is one of the essential precursor of GSLs biosynthesis. However, we also observed that photoreceptor (particularly, phyA) acts to inhibit GSLs via HY5–HDA9 module. Thus, it is likely that light modulates biosynthesis of GSLs to maintain proper daily amounts of GSLs by running both positive and negative control systems. In this aspect, we hypothesized that unidentified light-related factor(s) might play a positive role in the GSLs biosynthesis during light condition. It was well documented that daily amounts of GSLs exhibit a circadian rhythm. In consistent with previous studies, we observed that daily GSL biosynthesis exhibited circadian rhythm (Fig. 2, D to F). Thus, we reasoned that circadian rhythm regulator(s) during light period might play a positive impact on the biosynthesis of GSLs. For example, a recent study reported that GIGANTEA (GI), a circadian regulator, is required for the active biosynthesis of GSLs in *B. rapa* (Kim et al. 2021). To test this possibility, we examined whether *Arabidopsis* GI plays a positive role in the biosynthesis of GSLs in *Arabidopsis*. As shown in Supplementary Fig. S11C, amounts of GSLs were substantially reduced in *gi-1* mutant. It suggests that some circadian regulators including GI might play a positive role in the light-mediated regulation of GSLs in *Arabidopsis*. It would be an interesting future topic to examine the molecular mechanism on how light-related factors (i.e. circadian regulators) modulate GSLs biosynthetic pathway in *Arabidopsis*.

A recent study showed that HDA9 physically interacts with HY5 to modulate plant autophagy by targeting *ATG5* and *ATG8e* in *Arabidopsis* (Yang et al. 2020). In addition, HDA9 has been demonstrated to preferentially catalyze the removal of acetyl groups from the H3K9 and H3K27 histones of their target loci, resulting in the suppression of genes (Chen et al. 2016; Zheng et al. 2016). Furthermore, HDA9 is required for the recruitment of the PRC2 complex to *FLC* (Zeng et al. 2020). Another study showed that HDA9 and its related deacetylase HDA19 interact with DNA-binding TFs such as VAL1, VAL2 (Zeng et al. 2020), and PWR (Chen et al. 2016; Kim et al. 2016), suggesting that some histone deacetylases (HDACs) exhibit crosstalk with PRC2 via VAL1/2 TFs. In this study, we demonstrated that the G-box-binding HY5 physically associates with HDA9 to modulate the expression of GSL pathway genes. Thus, the recruitment of HDACs by DNA-binding TFs to repress specific target genes appears to be a conserved mechanism.

Understanding the molecular mechanisms underlying metabolite biosynthesis can enrich molecular breeding strategies for the development of elite crop varieties with improved quality. Recently, molecular breeding efforts have been made to exploit GSL metabolism to customize the GSL profiles of Brassicaceae crops (del Carmen Martinez-Ballesta et al. 2013; Ishida et al. 2014). A recent study reported that CCA1-OX plants exhibit increased indolic GSL levels, thus promoting aphid resistance (Lei et al. 2019). In this study, GSL biosynthesis was found to be most active in the morning for both aliphatic and indolic GSLs. Therefore, we believe that the light and circadian clock components are excellent candidate targets for molecular breeding to improve the quality of Brassicaceae crops.

Function of HY5–HDA9 module was previously investigated in terms of flowering time (Chu et al. 2022), salt stress (Yang et al. 2023), and autophagy response (Yang et al. 2022) in *Arabidopsis*. In this study, we now found that HY5 is actively involved in the regulation of secondary metabolism, GSLs which are related in the plant defense response against abiotic stresses (salt, drought, and wounding) as well as biotic stresses (herbivore attack). These findings may provide a strategy to develop stress-tolerant plants. In conclusion, our findings show that light signaling is crucially involved in controlling GSL biosynthesis in *Arabidopsis* plants. Our study provides insights into the molecular mechanisms underlying GSL biosynthesis, which involve HY5 and its interacting partner, HDA9.

Materials and methods

Plant materials and growth conditions

The Arabidopsis (*A. thaliana*) strain Col-0 was used as the genetic background for the WT, mutant, and transgenic lines. Seeds of *hy5-215* (Oyama et al. 1997) and *hda9-1* (Yang et al. 2020) mutants and transgenic lines harboring *p35S::HY5-GFP/hy5-215* have been previously described (Lee et al. 2011). *pHDA9::HDA9-FLAG/hda9-1* was generated by cloning the genomic region of *HDA9* containing ~1.2-kb promoter and coding sequence. Seeds were sterilized and placed on half-strength Murashige and Skoog agar. After 3 d of stratification at 4°C under dark conditions, *Arabidopsis* plants were grown in a growth room at 22°C under a LD condition (16-h light and 8-h dark).

RNA-Seq library preparation and sequencing

Three biological replicates and at least 10 seedlings per 1 replicate were collected for each sample and ground after freezing in liquid nitrogen for total RNA extraction. Total RNA was isolated from whole 1-wk-old *A. thaliana* seedlings grown under a LD condition using the RNeasy Plant Mini Kit (Qiagen, Hilden, Germany), following the manufacturer's instructions. The quantity and quality of the RNA were checked using a Nano-400 micro spectrophotometer (Allsheng Instrument Co., Hangzhou, China). Each complementary DNA (cDNA) library was prepared using the TruSeq Stranded mRNA LT Sample Prep Kit (Illumina, Inc., San Diego, CA, USA). Sequencing of the cDNA libraries was performed on an Illumina NovaSeq6000 platform using the paired-end sequencing protocol.

RNA-Seq data analysis

The FastQC program was used to assess the quality of the raw reads (www.bioinformatics.babraham.ac.uk/projects/fastqc). Raw reads were trimmed and qualitatively filtered before alignment (Bolger et al. 2014), and those exceeding a 90% threshold ($Q > 30$) were used for mapping. Trimmed reads of each sample were aligned to the *Arabidopsis* genome using TopHat2 with default parameters (Kim et al. 2013). Data from EnsemblPlants (https://plants.ensembl.org/Arabidopsis_thaliana/Info/Index) were used for the annotation of the *Arabidopsis* genome. Aligned reads were

converted to digital counts using FeatureCount (Liao et al. 2014). Differentially expressed genes in the Col-0 and *hy5-215* plants were identified using the EdgeR (Robinson et al. 2010). Cutoff and adjusted *P* values for the differential gene expression were set as ≥2-fold and ≤0.05, respectively. Multidimensional scaling plots and correlation heatmaps were generated using R packages (ver. 3.6.1; https://www.rstudio.com/products/rpackages/). The Venn diagrams were generated using the Venny web tool (ver. 2.1; https://bioinfogp.cnb.csic.es/tools/venny/). Heatmap analysis was performed using MeV (ver. 4.9.0). The aligned reads were converted into bigwig files for visualization using the Integrative Genomics Viewer program of the Broad Institute (Robinson et al. 2011).

RNA extraction and RT-qPCR analysis

One-wk-old seedlings grown under a LD condition were harvested at ZT4 and frozen in liquid nitrogen for total RNA extraction. Total RNA was extracted using a Spectrum Plant Total RNA Kit (Sigma-Aldrich, St. Louis, MO, USA) and treated with DNase I (New England Biolabs, Ipswich, MA, USA) to eliminate contaminating genomic DNA. Total RNAs (5 μg) were used for cDNA synthesis using the EasyScript reverse transcriptase enzyme (TransGen Biotech, Beijing, China). RT-qPCR was performed on a LineGene 9600 Plus (FQD-96A) Real-Time PCR Detection System (BioER, Hangzhou, China) using 2× Solg SYBR Green Mix (SolGent Co., Daejeon, Republic of Korea). Cycling conditions were as follows: 12 min at 95°C, and 45 cycles of 15 s at 95°C, 25 s at 60°C, and 35 s at 72°C. The qPCR values were normalized to the level of *PP2A* (AT1G13320) as a reference gene (Czechowski et al. 2005). RT-qPCR was performed with at least 3 biological replicates ($n = 3$). The primer sequences used for RT-qPCR amplification are listed in Supplementary Table S4.

ChIP-qPCR analysis

One-wk-old seedlings grown under a LD condition were harvested at the ZT4 time point, crosslinked in 1% formaldehyde solution, and then finely ground in liquid nitrogen. ChIP assays were performed as previously described (Kim and Sung 2017). Quantitative PCR was performed using 2× Solg SYBR Green Mix (SolGent, Republic of Korea) according to the manufacturer's instructions. The relative enrichment of each amplicon was first calculated based on a comparison with the Ct value of the input DNA sample. Next, the relative enrichment was calculated by comparison with each listed control region. All ChIP assays were performed with 3 technical replicates and at least 2 biological replicates. Real-time PCR was performed using a LineGene 9600 Plus (FQD-96A) Real-Time PCR Detection System (BioER). The primer sequences used for ChIP-qPCR analysis are listed in Supplementary Table S5.

Yeast two-hybrid assay

Full-length cDNA of *HY5* was cloned into the pGBKT7 vector in fusion with the GAL4 DNA-binding domain at the C-terminus, and *HDA9* was cloned into the pGADT7 vector in fusion with the GAL4 activation domain at the C-terminus. Primers used for cloning are listed in Supplementary Table S6. The constructs were transformed into yeast strains Y2HGold (for pGBKT7 constructs) and Y187 (for pGADT7 constructs) using a lithium acetate transformation method, according to the instructions of Yeastmaker Yeast Transformation System 2 (TaKaRa Bio, Kusatsu, Japan). The transformed yeast cells were plated onto synthetic dextrose without tryptophan (SD-Trp) or leucine (SD-Leu). After mating, yeast cells were first selected on SD-Trp-Leu plates, and the selected cells were plated on SD-His-Trp-Leu-Ade/X-gal/aureobasidin A to analyze protein–protein interactions. A total of 10 μL yeast cells with OD_{600} of 0.8 to 1.0 were grown for 4 d at 30°C.

Preparation of recombinant proteins

PCR-amplified cDNAs of *HDA9* and *HY5* were subcloned into pGEX 4T-1 and pCold TF (TaKaRa) with a strep tag at the C-terminus. The primers used for cloning are listed in Supplementary Table S6. *Escherichia coli* BL21(DE3)-CodonPlus cells harboring HDA9/pGEX 4T-1 and PIF3/pGEX 4T-1 (Shin et al. 2016) constructs were used to express HDA9 and PIF3 proteins with glutathione S-transferase (GST) and strep tag at their N- and C-termini, respectively. *E coli* BL21(DE3)-CodonPlus cells harboring HY5/pCold TF were used to express HY5 protein with 6× His and trigger factor tags at the N-terminus and a strep tag at the C-terminus. For the expression of recombinant proteins, *E. coli* cells were incubated at 37°C until OD_{600} reached 0.4 to 0.6 and then transferred to 20°C for pGEX 4T-1 constructs or 15°C for HY5/pCold TF constructs. After incubation at 20°C or 15°C for 1 h, isopropyl β-D-1-thiogalactopyranoside was added to a final concentration of 1 mM, and the culture was further incubated overnight. After cell harvesting and resuspension in ice-cold TE buffer (100 mM Tris, 1 mM EDTA, pH 8.0), protein extracts were obtained by sonication. After centrifugation, the supernatant was obtained and filtrated with a 0.45-μm syringe filter (Corning, Inc, Corning, NY, USA) to remove insoluble particles, and recombinant proteins (HDA9, PIF3, and HY5) were purified by streptavidin affinity chromatography (IBA Lifesciences, Germany).

Electrophoretic mobility shift assay

To assess the DNA-binding ability of AtHY5, we preformed EMSA following the method in a previous study (Hoang et al. 2021). TF-binding sites in the 1.0-kb upstream regions of 2 genes, *AtMYB29* and *AtIMD1*, were analyzed using PlantPAN 3.0, and found a G-box sequence (CACGTG) in each gene promoter. Then, 80-bp promoter fragments containing the G-box sequence were prepared as probes (Supplementary Table S7). The probes were labeled with ^{32}P-ATP using DNA 5′-End-Labeling System (Promega) and purified using the QIAquick Nucleotide Removal Kit (QIAGEN). 1 pmol of each ^{32}P-labeled probe was incubated with 2 μg of AtHY5 for 30 min in a 20-μL reaction mixture (50 mM Tris–HCl, pH 7.5, 50 mM NaCl, 200 mM KCl, 5 mM $MgCl_2$, 5 mM EDTA, 5 mM DTT, and 250 mM BSA). Cold competitor probes were generated from dimerized oligos without labeling. The reaction mixtures were resolved on 5% native polyacrylamide gels and dried under vacuum before autoradiography.

In vitro protein–protein interaction analysis

To examine the protein–protein interactions between HDA9 and HY5 in vitro, pull-down experiments were performed. His-TF/strep-fused HY5 (2 μg) and GST/strep-fused HDA9 or PIF3 (2 μg) were incubated for 60 min at 4°C in 500 μL of pull-down buffer (50 mM Tris–HCl, pH 7.5, 1 mM DTT, 150 mM NaCl, 0.6% (*w/v*) Tween-20, and 100 μg/mL BSA). Then, 40 μL of glutathione resin was added to each reaction and incubated for an additional 60 min. His-TF/strep-fused HY5 and GST/strep-fused HDA9 or PIF3 in the supernatant and precipitate were detected using electrochemiluminescence western blot substrates (Thermo Fisher Scientific, Waltham, MA, USA) with 1:3,000 GST-specific monoclonal antibodies (sc-138, Santa Cruz Biotechnology, Dallas, TX, USA) and 1:5,000 trigger factor-specific antibodies (M201, TaKaRa),

respectively. In this analysis, GST and PIF3 were used as negative and positive controls, respectively, for the interaction with HY5.

LCI assay

Full-length cDNAs of *HY5*, *HDA9*, and *PIF3* were PCR-amplified using the primer sets listed in Supplementary Table S6 and pCAMBIA1300-HY5:nLUC, pCAMBIA1300-cLUC:HDA9, and pCAMBIA1300-cLUC:PIF3. The constructs were transformed into *Agrobacterium tumefaciens* strain GV3101, and LCI assays were performed as previously described (Chen et al. 2008). Briefly, 2 d after *Agrobacterium* infiltration into 3-wk-old *N. benthamiana* leaves, luciferin working buffer (5 mM luciferin and 0.025% Triton X-100) was sprayed onto the leaves. After incubation for 5 min in the dark to quench the fluorescence, LUC images were captured using the G:BOX Chemi XL1.4 Imaging System (Syngene, Bangalore, India). An exposure time of 30 min with 2 × 2 binning was used for all the images. An empty vector (pCAMBIA1300-nLUC or pCAMBIA1300-cLUC) was used as a negative control, and pCAMBIA1300-cLUC:PIF3 was used as a positive control for the interaction with HY5.

Extraction and analysis of GSLs

Plant materials were harvested from 1-wk-old seedlings grown under a LD photoperiod (16 h). The fresh weights of all the seedlings were measured, and the seedlings were subsequently frozen in liquid nitrogen. Samples were ground into a fine powder for GSL analysis. GSLs were quantified using HPLC of the corresponding desulfo-glucosinolates (DS-GSLs). Briefly, lyophilized samples were incubated with 70% MeOH at 70°C for 20 min to inactivate myrosinase. The methanol extract was transferred into a polypropylene column (Thermo Fisher Scientific) and reacted with 11.25 units of sulfatase (Sigma-Aldrich) for 14 h at 37°C, with 0.5 mg/mL sinigrin (Sigma-Aldrich) used as the internal standard. Individual DS-GSLs were analyzed using a 3000 UHPLC System (Thermo Fisher Scientific). The DS-GSLs were separated on a C18 reverse-phase column (Zorbax XDB-C18, 4.6 × 250 mm, 5 μm particle size, Agilent Technologies, Santa Clara, CA, USA) with a water and acetonitrile gradient system. Samples (20 μL) were injected, and the flow rate was maintained at 1.0 mL min^{-1}. Peaks were identified using standard compounds (Phytoplan, Heidelberg, Germany), and sinigrin was used for relative quantification (Brown et al. 2003). The contents were analyzed independently with 3 replicates and presented as nmol/g on a fresh weight basis.

Analysis of GSLs by liquid chromatography coupled to diode array detection and electrospray ionization tandem mass spectrometry

The DS-GSLs analysis was performed using an Accela UHPLC system (Thermo Fisher Scientific) coupled with an ion-trap mass spectrometer (LTQ Velos Pro, Thermo Fisher Scientific). The samples (25 μl) were separated in C18 reverse-phase column (Zorbax XDB-C18, 4.6 × 250 mm, 5 μm particle size, Agilent) with a water and acetonitrile mobile phase and determined in negative-ion mode ([M-H]-). The MS operating conditions were as follows: capillary temperature (275°C), capillary voltage (5 kV), source heater temperature (250°C), sheath gas flow (35 arb), auxiliary gas flow (5 arb), and spectra scanning range (*m/z* 100 to 1,500). The molecular mass of DS-4OHB in *Arabidopsis* was identified according to a previous report (*m/z* 310, 356, and 621) (Kusznierewicz et al. 2013).

Statistical analysis

All statistical analyses in this study were performed using SAS (version 9.4; SAS Institute Inc., Cary, NC, USA). Statistical differences were calculated using one-way ANOVA. Values of $P < 0.05$ were considered significant, and the data are expressed as means ± SD of 3 biological replicates.

Accession numbers

The raw RNA-seq data used in this study were deposited in the NCBI Gene Expression Omnibus with the GEO accession code GSE250418. Accession numbers of genes in this study are given in Supplementary Table S8.

Acknowledgments

The authors thank Dr Caiji Gao at South China Normal University for providing the *hda9-1* mutants.

Author contributions

D.C. prepared all plant materials and performed genetic and molecular experiments. D.-M.C. performed the Y2H assay. S.-H.K conducted the split-luciferase assay. H.M. conducted HPLC analysis between Col-0 and *gi-1* mutant. J.-I.K. and D.-H.K. planned the experiments. D.C., J.-I.K., E.H., and D.-H.K. analyzed the data and wrote the manuscript. All authors have reviewed and approved the final manuscript for submission.

Supplementary data

The following materials are available in the online version of this article.

Supplementary Figure S1. UHPLC chromatogram of 1-wk-old *Arabidopsis* seedlings.

Supplementary Figure S2. Transcript levels of *CYP81F1* to *F4* genes in *Arabidopsis* seedlings.

Supplementary Figure S3. Contents of 4 individual GSLs in Col-0 and *hy5-215* from ZT0 to ZT20.

Supplementary Figure S4. GSL contents in Col-0 wild-type, *hy5-215* mutant, and *35S::HY5-GFP/hy5-215* transgenic plants.

Supplementary Figure S5. Transcriptome analysis identifying DEGs along the vernalization time course.

Supplementary Figure S6. Results of RT-qPCR analysis of 12 indolic GSL pathway genes in Col-0, *hy5-215*, and *35S::HY5-GFP/hy5-215* plants.

Supplementary Figure S7. Locations of the G-box (-CACGTG-) and ACGT motif (-ACGT-) in the genomic sequences of 12 DEGs involved in GSL biosynthesis in *Arabidopsis*.

Supplementary Figure S8. HY5 interacts with HDA9, a histone deacetylase.

Supplementary Figure S9. Enrichment of H3K27ac level on the genomic region of *MYB29* and *IMD1* between Col-0 and *hy5-215*.

Supplementary Figure S10. Transcript levels of 10 genes involved in the "secondary modification" phase from ZT0 to ZT22.

Supplementary Figure S11. Effect of different photoreceptors in GSLs biosynthesis.

Supplementary Table S1. Major GSLs identified by LC-ESI/MS from 1-wk-old *Arabidopsis* seedlings.

Supplementary Table S2. GSL content (nmol/g) in *Arabidopsis* seedlings grown under light and dark conditions.

Supplementary Table S3. Total and mapped reads to the *A. thaliana* reference genome using the Tophat2 alignment program.

Supplementary Table S4. List of primer sequences used for RT-qPCR analysis in this study.

Supplementary Table S5. List and sequences of ChIP-qPCR primers in this study

Supplementary Table S6. List and sequences of primers used for cloning in this study.

Supplementary Table S7. List and sequences of primers used for EMSA in this study.

Supplementary Table S8. Accession numbers of genes in this study.

Funding

This work was supported by the National Research Foundation grants funded by the Korean government (MSIT) (grant nos. 2021R1A5A1047822 to D.-H.K. and 2022R1A5A1031361 to J.-I.K.) and the National Science Foundation (MCB-2014408) to E.H.

Conflict of interest statement. None declared.

Data availability

The raw RNA-seq data used in this study were deposited in the NCBI Gene Expression Omnibus with the GEO accession code GSE250418.

References

Augustine R, Bisht NC. Biotic elicitors and mechanical damage modulate glucosinolate accumulation by co-ordinated interplay of glucosinolate biosynthesis regulators in polyploid Brassica juncea. *Phytochemistry*. 2015:117:43–50. https://doi.org/10.1016/j.phytochem.2015.05.015

Barillari J, Canistro D, Paolini M, Ferroni F, Pedulli GF, Iori R, Valgimigli L. Direct antioxidant activity of purified glucoerucin, the dietary secondary metabolite contained in rocket (Eruca sativa Mill.) seeds and sprouts. *J Agric Food Chem*. 2005:53(7):2475–2482. https://doi.org/10.1021/jf047945a

Blazevic I, Montaut S, Burcul F, Olsen CE, Burow M, Rollin P, Agerbirk N. Glucosinolate structural diversity, identification, chemical synthesis and metabolism in plants. *Phytochemistry*. 2020:169:112100. https://doi.org/10.1016/j.phytochem.2019.112100

Bolger AM, Lohse M, Usadel B. Trimmomatic: a flexible trimmer for Illumina sequence data. *Bioinformatics*. 2014:30(15):2114–2120. https://doi.org/10.1093/bioinformatics/btu170

Brown PD, Tokuhisa JG, Reichelt M, Gershenzon J. Variation of glucosinolate accumulation among different organs and developmental stages of *Arabidopsis thaliana*. *Phytochemistry*. 2003:62(3):471–481. https://doi.org/10.1016/s0031-9422(02)00549-6

Burko Y, Seluzicki A, Zander M, Pedmale UV, Ecker JR, Chory J. Chimeric activators and repressors define HY5 activity and reveal a light-regulated feedback mechanism. *Plant Cell*. 2020:32(4):967–983. https://doi.org/10.1105/tpc.19.00772

Celenza JL, Quiel JA, Smolen GA, Merrikh H, Silvestro AR, Normanly J, Bender J. The Arabidopsis ATR1 Myb transcription factor controls indolic glucosinolate homeostasis. *Plant Physiol*. 2005:137(1):253–262. https://doi.org/10.1104/pp.104.054395

Chen HM, Zou Y, Shang YL, Lin HQ, Wang YJ, Cai R, Tang XY, Zhou JM. Firefly luciferase complementation imaging assay for protein-protein interactions in plants. *Plant Physiol*. 2008:146(2):368–376. https://doi.org/10.1104/pp.107.111740

Chen X, Lu L, Mayer KS, Scalf M, Qian S, Lomax A, Smith LM, Zhong X. POWERDRESS interacts with HISTONE DEACETYLASE 9 to promote aging in Arabidopsis. *Elife*. 2016:5:e17214. https://doi.org/10.7554/eLife.17214

Chu L, Yang C, Zhuang F, Gao Y, Luo M. The HDA9-HY5 module epigenetically regulates flowering time in Arabidopsis thaliana. *J Cell Physiol*. 2022:237(7):2961–2968. https://doi.org/10.1002/jcp.30761

Czechowski T, Stitt M, Altmann T, Udvardi MK, Scheible WR. Genome-wide identification and testing of superior reference genes for transcript normalization in Arabidopsis. *Plant Physiol*. 2005:139(1):5–17. https://doi.org/10.1104/pp.105.063743

del Carmen Martinez-Ballesta M, Moreno DA, Carvajal M. The physiological importance of glucosinolates on plant response to abiotic stress in brassica. *Int J Mol Sci*. 2013:14(6):11607–11625. https://doi.org/10.3390/ijms140611607

Fahey JW, Wehage SL, Holtzclaw WD, Kensler TW, Egner PA, Shapiro TA, Talalay P. Protection of humans by plant glucosinolates: efficiency of conversion of glucosinolates to isothiocyanates by the gastrointestinal microflora. *Cancer Prev Res (Phila)*. 2012:5(4):603–611. https://doi.org/10.1158/1940-6207.CAPR-11-0538

Fahey JW, Zalcmann AT, Talalay P. The chemical diversity and distribution of glucosinolates and isothiocyanates among plants. *Phytochemistry*. 2001:56(1):5–51. https://doi.org/10.1016/s0031-9422(00)00316-2

Farquharson KL. A plastidic transporter involved in aliphatic glucosinolate biosynthesis. *Plant Cell*. 2009:21(6):1622. https://doi.org/10.1105/tpc.109.210611

Fuentes F, Paredes-Gonzalez X, Kong AN. Dietary glucosinolates sulforaphane, phenethyl isothiocyanate, indole-3-carbinol/3,3′-diindolylmethane: anti-oxidative stress/inflammation, Nrf2, epigenetics/epigenomics and in vivo cancer chemopreventive efficacy. *Curr Pharmacol Rep*. 2015:1(3):179–196. https://doi.org/10.1007/s40495-015-0017-y

Gigolashvili T, Engqvist M, Yatusevich R, Muller C, Flugge UI. HAG2/MYB76 and HAG3/MYB29 exert a specific and coordinated control on the regulation of aliphatic glucosinolate biosynthesis in Arabidopsis thaliana. *New Phytol*. 2008:177(3):627–642. https://doi.org/10.1111/j.1469-8137.2007.02295.x

Gigolashvili T, Yatusevich R, Berger B, Muller C, Flugge UI. The R2R3-MYB transcription factor HAG1/MYB28 is a regulator of methionine-derived glucosinolate biosynthesis in Arabidopsis thaliana. *Plant J*. 2007:51(2):247–261. https://doi.org/10.1111/j.1365-313X.2007.03133.x

Grubb CD, Abel S. Glucosinolate metabolism and its control. *Trends Plant Sci*. 2006:11(2):89–100. https://doi.org/10.1016/j.tplants.2005.12.006

Halkier BA, Gershenzon J. Biology and biochemistry of glucosinolates. *Annu Rev Plant Biol*. 2006:57(1):303–333. https://doi.org/10.1146/annurev.arplant.57.032905.105228

Hansen BG, Kerwin RE, Ober JA, Lambrix VM, Mitchell-Olds T, Gershenzon J, Halkier BA, Kliebenstein DJ. A novel 2-oxoacid-dependent dioxygenase involved in the formation of the goiterogenic 2-hydroxybut-3-enyl glucosinolate and generalist insect resistance in Arabidopsis. *Plant Physiol*. 2008:148(4):2096–2108. https://doi.org/10.1104/pp.108.129981

Hecht SS. Inhibition of carcinogenesis by isothiocyanates. *Drug Metab Rev*. 2000:32(3-4):395–411. https://doi.org/10.1081/dmr-100102342

Hirai MY, Sugiyama K, Sawada Y, Tohge T, Obayashi T, Suzuki A, Araki R, Sakurai N, Suzuki H, Aoki K, *et al*. Omics-based identification of Arabidopsis Myb transcription factors regulating aliphatic glucosinolate biosynthesis. *Proc Natl Acad Sci U S A*. 2007:104(15):6478–6483. https://doi.org/10.1073/pnas.0611629104

Hoang QTN, Tripathi S, Cho JY, Choi DM, Shin AY, Kwon SY, Han YJ, Kim JI. Suppression of phytochrome-interacting factors enhances photoresponses of seedlings and delays flowering with increased

plant height in Brachypodium distachyon. *Front Plant Sci*. 2021:12:756795. https://doi.org/10.3389/fpls.2021.756795

Huseby S, Koprivova A, Lee BR, Saha S, Mithen R, Wold AB, Bengtsson GB, Kopriva S. Diurnal and light regulation of sulphur assimilation and glucosinolate biosynthesis in Arabidopsis. *J Exp Bot*. 2013:64(4):1039–1048. https://doi.org/10.1093/jxb/ers378

Ishida M, Hara M, Fukino N, Kakizaki T, Morimitsu Y. Glucosinolate metabolism, functionality and breeding for the improvement of Brassicaceae vegetables. *Breed Sci*. 2014:64(1):48–59. https://doi.org/10.1270/jsbbs.64.48

Jung JH, Domijan M, Klose C, Biswas S, Ezer D, Gao M, Khattak AK, Box MS, Charoensawan V, Cortijo S, *et al*. Phytochromes function as thermosensors in Arabidopsis. *Science*. 2016:354(6314):886–889. https://doi.org/10.1126/science.aaf6005

Kim D, Pertea G, Trapnell C, Pimentel H, Kelley R, Salzberg SL. TopHat2: accurate alignment of transcriptomes in the presence of insertions, deletions and gene fusions. *Genome Biol*. 2013:14(4):R36. https://doi.org/10.1186/gb-2013-14-4-r36

Kim DH, Sung S. The binding specificity of the PHD-finger domain of VIN3 moderates vernalization response. *Plant Physiol*. 2017:173(2):1258–1268. https://doi.org/10.1104/pp.16.01320

Kim NS, Kim SJ, Jo JS, Lee JG, Lee SI, Kim DH, Kim JA. The BrGI circadian clock gene is involved in the regulation of glucosinolates in Chinese cabbage. *Genes (Basel)*. 2021:12(11). https://doi.org/10.3390/genes12111664

Kim YJ, Wang R, Gao L, Li D, Xu C, Mang H, Jeon J, Chen X, Zhong X, Kwak JM, *et al*. POWERDRESS and HDA9 interact and promote histone H3 deacetylation at specific genomic sites in Arabidopsis. *Proc Natl Acad Sci U S A*. 2016:113(51):14858–14863. https://doi.org/10.1073/pnas.1618618114

Klein M, Reichelt M, Gershenzon J, Papenbrock J. The three desulfoglucosinolate sulfotransferase proteins in Arabidopsis have different substrate specificities and are differentially expressed. *FEBS J*. 2006:273(1):122–136. https://doi.org/10.1111/j.1742-4658.2005.05048.x

Kliebenstein DJ, Lambrix VM, Reichelt M, Gershenzon J, Mitchell-Olds T. Gene duplication in the diversification of secondary metabolism: tandem 2-oxoglutarate-dependent dioxygenases control glucosinolate biosynthesis in Arabidopsis. *Plant Cell*. 2001:13(3):681–693. https://doi.org/10.1105/tpc.13.3.681

Koprivova A, Kopriva S. Molecular mechanisms of regulation of sulfate assimilation: first steps on a long road. *Front Plant Sci*. 2014:5:589. https://doi.org/10.3389/fpls.2014.00589

Kusznierewicz B, Iori R, Piekarska A, Namiesnik J, Bartoszek A. Convenient identification of desulfoglucosinolates on the basis of mass spectra obtained during liquid chromatography-diode array-electrospray ionisation mass spectrometry analysis: method verification for sprouts of different Brassicaceae species extracts. *J Chromatogr A*. 2013:1278:108–115. https://doi.org/10.1016/j.chroma.2012.12.075

Lee BR, Koprivova A, Kopriva S. The key enzyme of sulfate assimilation, adenosine 5′-phosphosulfate reductase, is regulated by HY5 in Arabidopsis. *Plant J*. 2011:67(6):1042–1054. https://doi.org/10.1111/j.1365-313X.2011.04656.x

Lei JX, Jayaprakasha GK, Singh J, Uckoo R, Borrego EJ, Finlayson S, Kolomiets M, Patil BS, Braam J, Zhu-Salzmana K. CIRCADIAN CLOCK-ASSOCIATED1 controls resistance to aphids by altering indole glucosinolate production. *Plant Physiol*. 2019:181(3):1344–1359. https://doi.org/10.1104/pp.19.00676

Liao Y, Smyth GK, Shi W. featureCounts: an efficient general purpose program for assigning sequence reads to genomic features. *Bioinformatics*. 2014:30(7):923–930. https://doi.org/10.1093/bioinformatics/btt656

Malitsky S, Blum E, Less H, Venger I, Elbaz M, Morin S, Eshed Y, Aharoni A. The transcript and metabolite networks affected by the two clades of Arabidopsis glucosinolate biosynthesis regulators. *Plant Physiol*. 2008:148(4):2021–2049. https://doi.org/10.1104/pp.108.124784

Mikkelsen MD, Petersen BL, Olsen CE, Halkier BA. Biosynthesis and metabolic engineering of glucosinolates. *Amino Acids*. 2002:22(3):279–295. https://doi.org/10.1007/s007260200014

Mitreiter S, Gigolashvili T. Regulation of glucosinolate biosynthesis. *J Exp Bot*. 2021:72(1):70–91. https://doi.org/10.1093/jxb/eraa479

Neal CS, Fredericks DP, Griffiths CA, Neale AD. The characterisation of AOP2: a gene associated with the biosynthesis of aliphatic alkenyl glucosinolates in Arabidopsis thaliana. *BMC Plant Biol*. 2010:10(1):170. https://doi.org/10.1186/1471-2229-10-170

Oyama T, Shimura Y, Okada K. The Arabidopsis HY5 gene encodes a bZIP protein that regulates stimulus-induced development of root and hypocotyl. *Genes Dev*. 1997:11(22):2983–2995. https://doi.org/10.1101/gad.11.22.2983

Petersen A, Hansen LG, Mirza N, Crocoll C, Mirza O, Halkier BA. Changing substrate specificity and iteration of amino acid chain elongation in glucosinolate biosynthesis through targeted mutagenesis of Arabidopsis methylthioalkylmalate synthase 1. *Biosci Rep*. 2019:39(7):BSR20190446. https://doi.org/10.1042/BSR20190446

Pfalz M, Mikkelsen MD, Bednarek P, Olsen CE, Halkier BA, Kroymann J. Metabolic engineering in Nicotiana benthamiana reveals key enzyme functions in Arabidopsis indole glucosinolate modification. *Plant Cell*. 2011:23(2):716–729. https://doi.org/10.1105/tpc.110.081711

Rask L, Andreasson E, Ekbom B, Eriksson S, Pontoppidan B, Meijer J. Myrosinase: gene family evolution and herbivore defense in Brassicaceae. *Plant Mol Biol*. 2000:42(1):93–113. https://doi.org/10.1023/A:1006380021658

Robinson JT, Thorvaldsdottir H, Winckler W, Guttman M, Lander ES, Getz G, Mesirov JP. Integrative genomics viewer. *Nat Biotechnol*. 2011:29(1):24–26. https://doi.org/10.1038/nbt.1754

Robinson MD, Mccarthy DJ, Smyth GK. edgeR: a Bioconductor package for differential expression analysis of digital gene expression data. *Bioinformatics*. 2010:26(1):139–140. https://doi.org/10.1093/bioinformatics/btp616

Schuster J, Knill T, Reichelt M, Gershenzon J, Binder S. Branched-chain aminotransferase4 is part of the chain elongation pathway in the biosynthesis of methionine-derived glucosinolates in Arabidopsis. *Plant Cell*. 2006:18(10):2664–2679. https://doi.org/10.1105/tpc.105.039339

Shin AY, Han YJ, Baek A, Ahn T, Kim SY, Nguyen TS, Son M, Lee KW, Shen Y, Song PS, *et al*. Evidence that phytochrome functions as a protein kinase in plant light signalling. *Nat Commun*. 2016:7(1):11545. https://doi.org/10.1038/ncomms11545

Sonderby IE, Geu-Flores F, Halkier BA. Biosynthesis of glucosinolates–gene discovery and beyond. *Trends Plant Sci*. 2010:15(5):283–290. https://doi.org/10.1016/j.tplants.2010.02.005

Sonderby IE, Hansen BG, Bjarnholt N, Ticconi C, Halkier BA, Kliebenstein DJ. A systems biology approach identifies a R2R3 MYB gene subfamily with distinct and overlapping functions in regulation of aliphatic glucosinolates. *PLoS One*. 2007:2(12):e1322. https://doi.org/10.1371/journal.pone.0001322

Yang C, Shen W, Yang L, Sun Y, Li X, Lai M, Wei J, Wang C, Xu Y, Li F, *et al*. HY5-HDA9 module transcriptionally regulates plant autophagy in response to light-to-dark conversion and nitrogen starvation. *Mol Plant*. 2020:13(3):515–531. https://doi.org/10.1016/j.molp.2020.02.011

Yang C, Shen W, Yang L, Sun Y, Li X, Lai M, Wei J, Wang C, Xu Y, Li F, *et al.* HY5-HDA9 module transcriptionally regulates plant autophagy in response to light-to-dark conversion and nitrogen starvation. *Mol Plant*. 2022:15(10):1632–1634. https://doi.org/10.1016/j.molp.2022.09.015

Yang J, Qu X, Li T, Gao Y, Du H, Zheng L, Ji M, Zhang P, Zhang Y, Hu J, *et al.* HY5-HDA9 orchestrates the transcription of HsfA2 to modulate salt stress response in Arabidopsis. *J Integr Plant Biol*. 2023:65(1):45–63. https://doi.org/10.1111/jipb.13372

Zeng X, Gao Z, Jiang C, Yang Y, Liu R, He Y. HISTONE DEACETYLASE 9 functions with polycomb silencing to repress FLOWERING LOCUS C expression. *Plant Physiol*. 2020:182(1):555–565. https://doi.org/10.1104/pp.19.00793

Zheng Y, Ding Y, Sun X, Xie S, Wang D, Liu X, Su L, Wei W, Pan L, Zhou DX. Histone deacetylase HDA9 negatively regulates salt and drought stress responsiveness in Arabidopsis. *J Exp Bot*. 2016:67(6):1703–1713. https://doi.org/10.1093/jxb/erv562